THE RECEIVING SYSTEM OF A DUAL DYE LIDAR TO STUDY MOLECULAR AND AEROSOL DENSITIES AT THE BASE OF THE STRATOSPHERE

by

John Dexter Davidson, Junior

A Thesis Submitted to the Faculty of the

DEPARTMENT OF ATMOSPHERIC SCIENCE

In Partial Fulfillment of the Requirements

For the Degree of

MASTER OF SCIENCE

In the Graduate College

THE UNIVERSITY OF ARIZONA

1989

REPORT DOCUMENTATION PAGE

Form Approved
OMB No. 0704-0188

1a. REPORT SECURITY CLASSIFICATION UNCLASSIFIED	1b. RESTRICTIVE MARKINGS NONE
2a. SECURITY CLASSIFICATION AUTHORITY	3. DISTRIBUTION/AVAILABILITY OF REPORT APPROVED FOR PUBLIC RELEASE; DISTRIBUTION UNLIMITED.
2b. DECLASSIFICATION/DOWNGRADING SCHEDULE	
4. PERFORMING ORGANIZATION REPORT NUMBER(S)	5. MONITORING ORGANIZATION REPORT NUMBER(S) AFIT/CI/CIA-89-073
6a. NAME OF PERFORMING ORGANIZATION AFIT STUDENT AT UNIV OF ARIZONA 6b. OFFICE SYMBOL (If applicable)	7a. NAME OF MONITORING ORGANIZATION AFIT/CIA
6c. ADDRESS (City, State, and ZIP Code)	7b. ADDRESS (City, State, and ZIP Code) Wright-Patterson AFB OH 45433-6583
8a. NAME OF FUNDING/SPONSORING ORGANIZATION 8b. OFFICE SYMBOL (If applicable)	9. PROCUREMENT INSTRUMENT IDENTIFICATION NUMBER
8c. ADDRESS (City, State, and ZIP Code)	10. SOURCE OF FUNDING NUMBERS PROGRAM ELEMENT NO. / PROJECT NO. / TASK NO. / WORK UNIT ACCESSION NO.

11. TITLE (Include Security Classification) (UNCLASSIFIED)
The Receiving System of a Dual Dye Lidar to Study Molecular and Aerosol Densities at the Base of the Stratosphere

12. PERSONAL AUTHOR(S)
John Dexter Davidson, Junior

13a. TYPE OF REPORT	13b. TIME COVERED	14. DATE OF REPORT (Year, Month, Day)	15. PAGE COUNT
THESIS/DISSERTATION	FROM _____ TO _____	1989	60

16. SUPPLEMENTARY NOTATION
APPROVED FOR PUBLIC RELEASE IAW AFR 190-1
ERNEST A. HAYGOOD, 1st Lt, USAF
Executive Officer, Civilian Institution Programs

17. COSATI CODES			18. SUBJECT TERMS (Continue on reverse if necessary and identify by block number)
FIELD	GROUP	SUB-GROUP	

19. ABSTRACT (Continue on reverse if necessary and identify by block number)

20. DISTRIBUTION/AVAILABILITY OF ABSTRACT ☒ UNCLASSIFIED/UNLIMITED ☐ SAME AS RPT. ☐ DTIC USERS	21. ABSTRACT SECURITY CLASSIFICATION UNCLASSIFIED
22a. NAME OF RESPONSIBLE INDIVIDUAL ERNEST A. HAYGOOD, 1st Lt, USAF	22b. TELEPHONE (Include Area Code) (513) 255-2259 22c. OFFICE SYMBOL AFIT/CI

THE RECEIVING SYSTEM OF A DUAL DYE LIDAR TO STUDY MOLECULAR AND AEROSOL DENSITIES AT THE BASE OF THE STRATOSPHERE

by

John Dexter Davidson, Junior

A Thesis Submitted to the Faculty of the

DEPARTMENT OF ATMOSPHERIC SCIENCE

In Partial Fulfillment of the Requirements

For the Degree of

MASTER OF SCIENCE

In the Graduate College

THE UNIVERSITY OF ARIZONA

1989

STATEMENT BY AUTHOR

This thesis has been submitted in partial fulfillment of requirements for an advanced degree at the University of Arizona and is deposited in the University Library to be made available to borrowers under rules of the library.

Brief quotations from this thesis are allowable without special permission, provided that accurate acknowledgement of source is made. Requests for permission for extended quotation from or reproduction of this manuscript in whole or in part may be granted by the head of the major department or the Dean of the Graduate College when in his or her judgment the proposed use of the material is in the interests of scholarship. In all other instances, however, permission must be obtained from the author.

SIGNED: John D. Davidson Jr.

APPROVAL BY THESIS DIRECTOR

This thesis has been approved on the date shown below:

R.M. Schotland

R.M. SCHOTLAND
Professor of Atmospheric Sciences

6 June 1989
Date

ACKNOWLEDGEMENTS

I wish to express my deepest gratitude to Dr Richard M. Schotland for his guidance and encouragement throughout the course of this project.

I am also grateful to Mr Richard Milliron for the skillful machining of the many mechanical parts and for his considerate advice. Also, Mr Andrew Hudor for his help in building and wiring the electronic interfaces for control circuits.

Finally, I wish to thank Dr David Winker for his thoughtful advice and careful review of this thesis.

TABLE OF CONTENTS

TABLE OF CONTENTS – – Continued

LIST OF ILLUSTRATIONS

ABSTRACT

The operating principles and design of an optical receiver for a Light Detection and Ranging (LIDAR) remote sensing instrument are addressed. The performance and limitations of a biaxial monostatic LIDAR system utilizing this design are investigated.

The complete optical and structural design of the receiver, including specifications of components are outlined. The thermal stabilization of the detector assembly and the integration of control electronics are described. A detailed discussion of alignment procedures and possible improvements are made. A sample observation is presented with suggestions for fully automating the system.

CHAPTER 1

INTRODUCTION

The measurement of atmospheric constituents and their motion plays an integral part in the understanding of the Earth-Biosphere interaction. The distances across which accurate measurements must be made are extremely large. Hence, in situ measurements are generally inadequate or impossible to make. This circumstance has resulted in rapid growth within the field of remote sensing. Remote sensing systems may passively collect electromagnetic or acoustic waves transmitted from a distant point, or they may illuminate a volume of the atmosphere with radiation and observe the backscattered signal. These instruments operate over the entire spectrum from gamma waves to extremely low frequency radio waves.

This thesis is concerned with the design and the construction of the optical receiver of a remote sensing instrument called a LIDAR, for light detection and ranging.

The Experiment

The project in which this optical receiver is to be utilized has as a goal the observation of laser radiation which is backscattered from molecules and aerosols located at altitudes from ground level to the base of the stratosphere. This objective and the LIDAR components form the basis for all design considerations. The furnished LIDAR components were a

dye laser, a 30-inch primary mirror, and a photomultiplier tube (PMT). These elements established the primary set of constraints on the design of the optical receiver.

A second constraint was established by the geometry of the laser laboratory and the portion of the roof where the primary mirror would be mounted (Figure 1.1). The laser laboratory is located on the top floor of the Physics and Atmospheric Sciences Building and include a hatch in the roof above the laser. The primary mirror was mounted on the roof approximately seven feet to the northeast of the hatch. The major impact of this geometry is to complicate the alignment procedure for the transmitter and receiver optic axes. This problem is addressed in Appendix A.

Design efforts are best directed if the goal can be broken down into smaller tasks. In the course of conducting this experiment, the work was separated into three primary tasks:

1. Radiation of the stratosphere with a collimated laser pulse from the dye laser.
2. Collection of the backscattered laser radiation from the atmosphere.
3. Measurement of the backscattered signal as a function of altitude.

The first task was simplified since a prior project (Alejandro, 1983) provided the dye laser for this LIDAR application. The laser beam was routed through a hatch in the roof above the laser by a directing mirror mounted on a three-point adjustable mount.

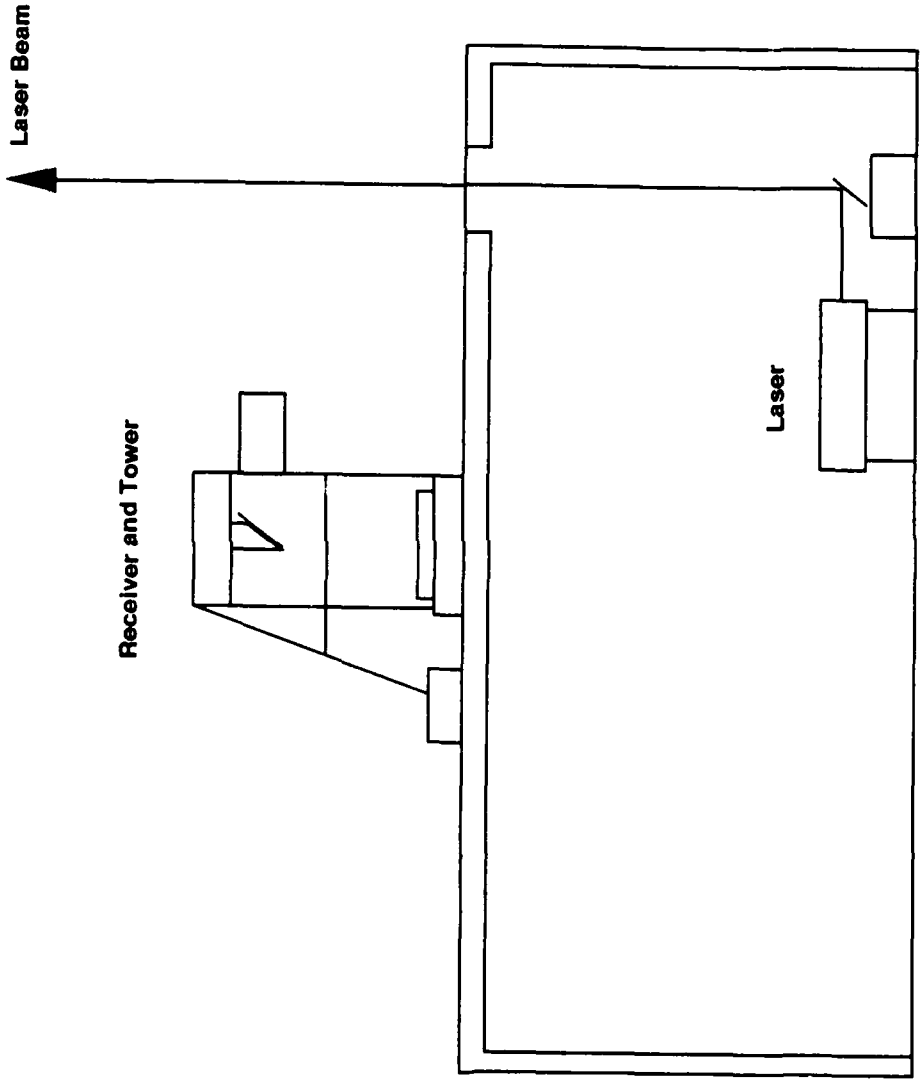

Figure 1.1 Laser Laboratory and Roof

The second task deals with the optical receiver. A LIDAR receiver has two parts, a collector and a detector. The collector receives incoming radiation within its field of view and transmits this signal through a selected bandpass filter to the detector. The optical elements of the receiver are specified on the basis of geometric considerations and image quality. The optical design of the receiver was simplified since it was not intended as an imaging system. Instead, the total flux incident upon the mirror is measured as a function of time.

The third and final task was to extract the signal output from the photomultiplier tube and display the backscattered signal. This was accomplished by viewing the output of the PMT on an oscilloscope. On the display, voltage amplitude represents scattering cross section, and time is translated into altitude by the LIDAR equation. A discussion of the LIDAR equation in Chapter 2 gives a more detailed explanation of how the return signal is treated. A digital data processing system has been developed for this LIDAR by Wissell (1983).

Optical Receiver Design

Design of the optical receiver was divided into two steps, the optical system layout and the structural design. The layout of the optical system provides the dimensional guidelines for the structural design, and must be pursued first. Figure 1.2 is a diagram of the optical elements required in the receiver.

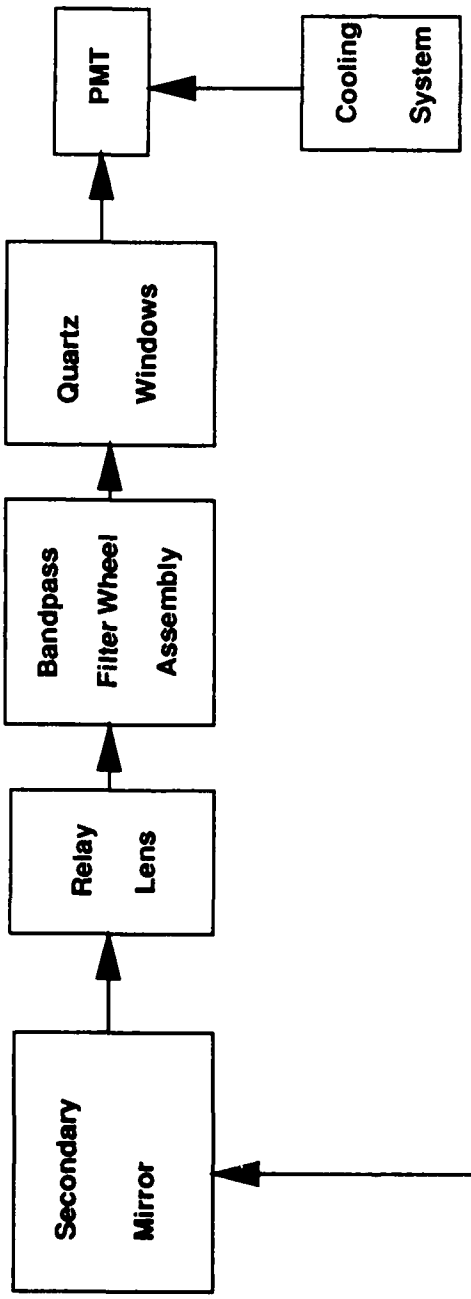

Figure 1.2 Block Diagram of Optical System

The optical design goal is to focus all of the backscattered laser energy collected by the primary mirror onto the cathode of the photomultiplier tube and to minimize any background radiation. This optical system includes a secondary mirror and a relay lens which are designed to image the surface of the primary mirror onto the full active region of the PMT cathode. An even distribution of light across the cathode diminishes the effect of variable response by the cathode often encountered by a focused spot.

Backscattered laser light collected by the primary mirror is directed vertically to a 5 X 7 inch secondary mirror. The secondary mirror is centered on the optic axis 72 inches above the primary mirror and at an angle of 45 degrees to the vertical. Thus the focal point of the primary mirror is located two feet from the vertical axis. This ensures that the detector assembly will be sufficiently beyond the field of view of the primary mirror to prevent obscuration. Only the secondary mirror and its mounting bracket occult the primary mirror (approximately 5%). This is much less than the detector assembly would cause if it were mounted directly overhead (approximately 20%).

Normally a field lens is placed at the focal point of the primary mirror. The chief rays (C.R.) then determine the distance between the field lens and the detector (Figure 1.3). That design is not feasible for this system because of the dimensions of the intervening optical elements. A narrow bandpass filter is used to reduce the spectral range of the receiver and two quartz windows thermally isolate the PMT chamber. These are each one

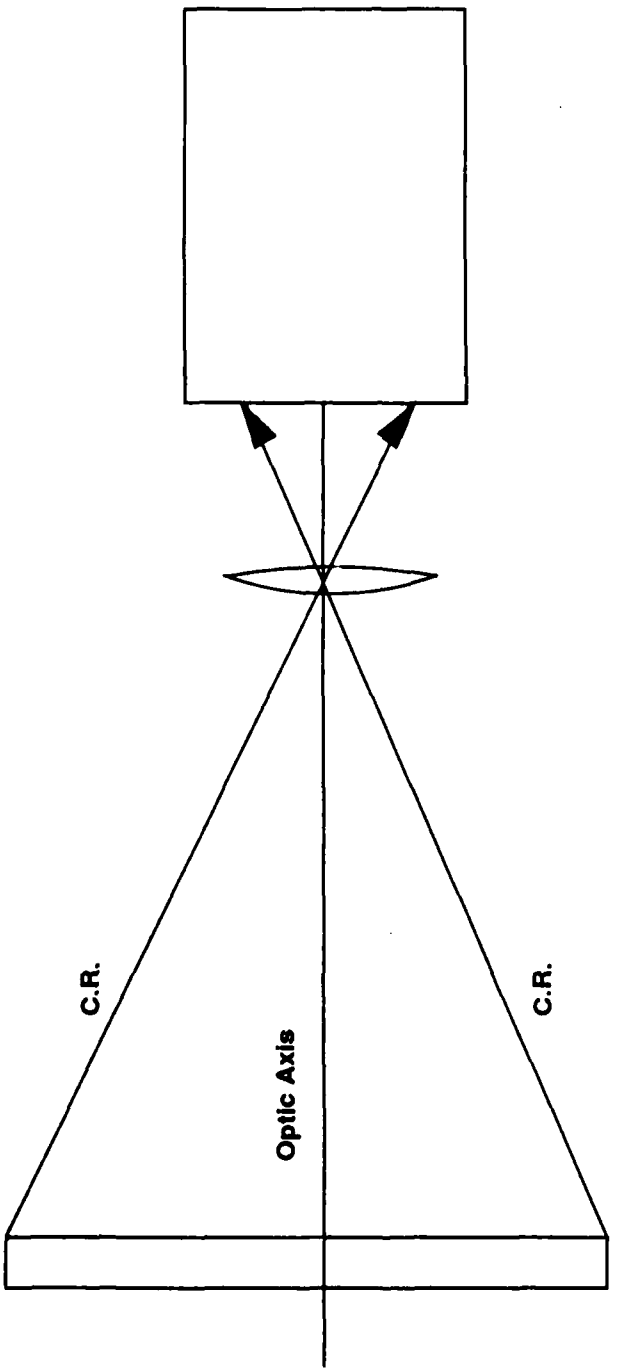

Figure 1.3 Field Lens at Focal Point of Primary

inch in diameter and would significantly occult the beam from the primary mirror. The solution was to position the field lens, now a relay lens, with its focal point beyond the focal point of the primary mirror (Figure 1.4).

The relay lens is a planar convex quartz lens with a 100 millimeter focal length. It is centered on the optic axis approximately 118 inches from the primary mirror. In this arrangement, quartz window "E" is a fixed field stop for the system restricting the field of view to 9 milliradians. The backscattered laser radiation within this field of view is spread across a 0.65 inch radius circle on the center of the PMT cathode. The total active region of the PMT cathode is 0.85 inches in radius. A series of fixed stops may be placed in front of the relay lens to further reduce the field of view of the receiver.

Structural considerations consisted primarily of designing a framework that would withstand normal environmental stresses, such as strong winds and heavy rains. Secondly, easy access to the optical elements and the mounting brackets with sufficient alignment capability were needed. Pre-punched angle iron was used to build a frame around the primary mirror. This gave a combination of structural integrity and easy access to components.

Figure 1.5 is a diagram of the final design. All metal surfaces were primed and then painted white. This prevents corrosion and keeps the surface temperatures cooler during the hot Tucson summer. Chapters 4 and 5 go through the actual steps to implement this design.

Figure 1.4 Optical Receiver with Relay Lens

Component	Description
A	Primary Mirror
B	Relay Lens
C	Bandpass Filter
D	Quartz Window
E	Quartz Window
F	Photomultiplier Tube

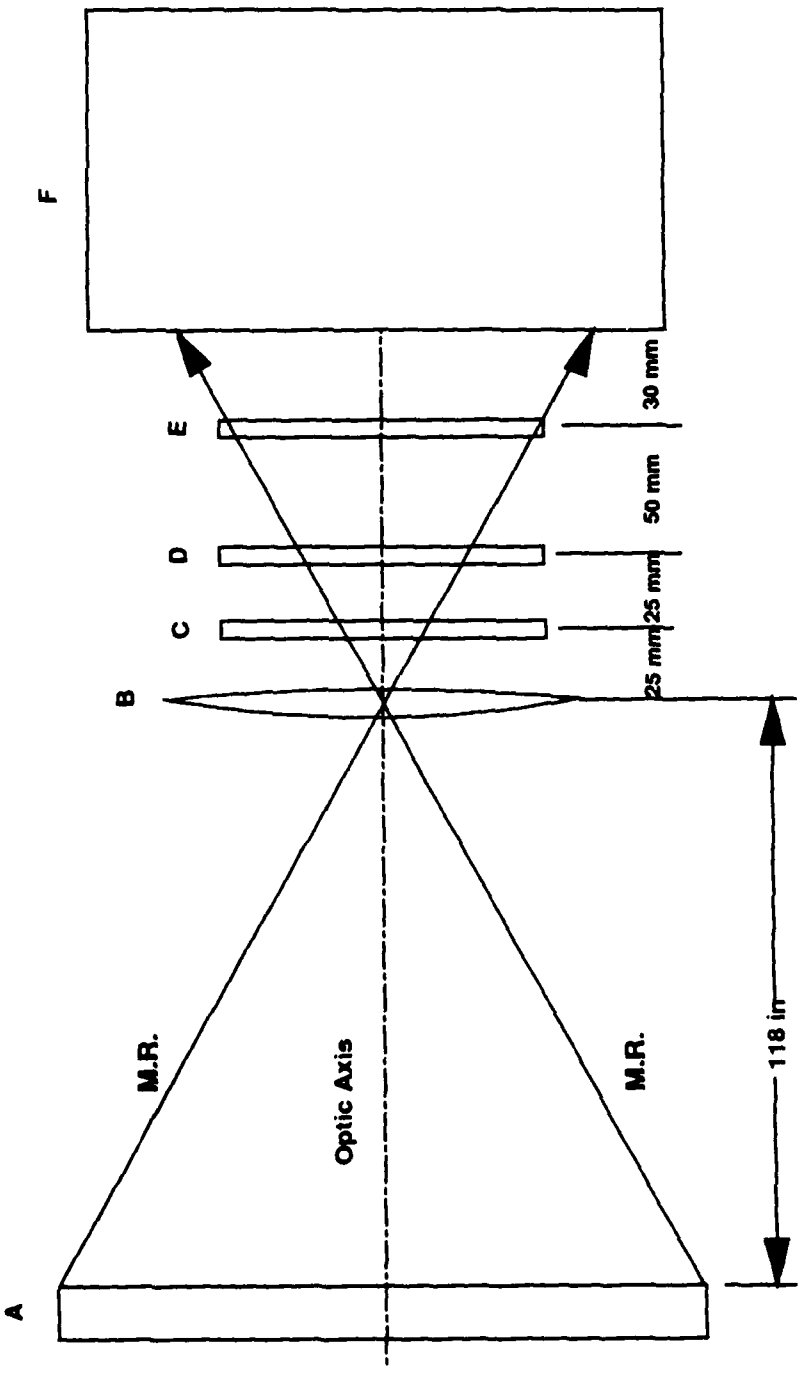

Figure 1.4 Optical Receiver with Relay Lens

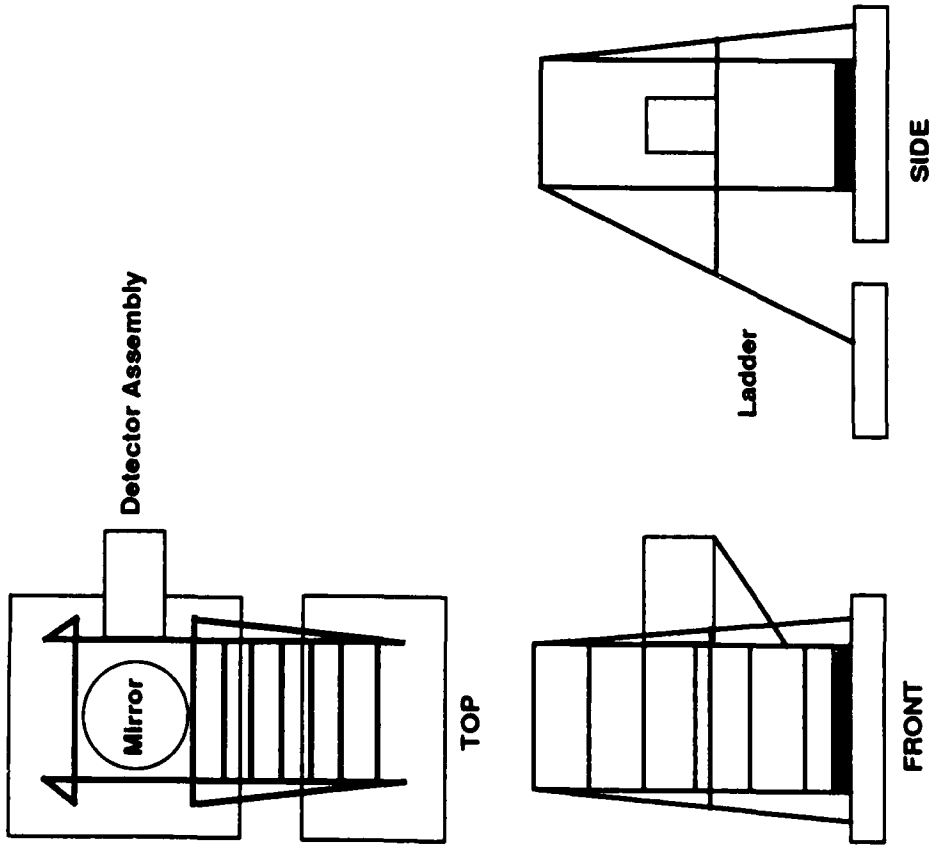

Figure 1.5 Diagram of Final Tower Design

CHAPTER 2

LIDAR

A class of remote sensing instruments called LIDAR propagate laser radiation through the atmosphere and observe the backscattered signal with an optical receiver. Within the remote sensing field, lasers have advanced research by quantum leaps. The precision with which a laser can probe the atmosphere is fundamental to these advances, and a direct consequence of the laser's exceptional temporal and spatial coherence. At visible wavelengths, the laser's bandwidth is on the order of one tenth of one Angstrom. This allows us to investigate molecular distributions by selectively radiating the atmosphere at the wavelength of individual absorption lines.

Another characteristic of the laser is that its radiation is highly directional. That is, the laser beam has a very small angular divergence. This can be seen by observing the scattering from smoke blown into the path of a laser beam. This narrow divergence allows us to be very precise about where we are pointing the beam in the atmosphere.

LIDAR operates on the same basic principle as does a radar, but at much shorter wavelengths. Like a radar, there is both a transmitter and a receiver, with a variety of configurations for the receiver in relation to the transmitter. The configuration used in this experiment is called a biaxial, monostatic LIDAR.

Biaxial Monostatic LIDAR System

The principle components of a monostatic LIDAR are depicted in Figure 2.1. The transmitter and the receiver do not have a common optic axis (coaxial). Instead, the transmitter's exit and the receiver's entrance optical elements are positioned relatively close to each other with their optic axes aligned parallel (biaxial). The near range limit of this configuration is the region where the two beams overlap. Therefore, it is advantageous to have the shortest possible horizontal distance between the two axes.

The output of the transmitter's laser cavity is collimated before the beam is directed into the sky. Collimation further reduces the angular spread or divergence of the beam as it propagates through the atmosphere. This provides greater horizontal resolution by illuminating a smaller sampling volume. Notice that the field of view of the receiver is larger than the beam spread of the transmitter. Once the system is aligned, the field of view of the receiver may be stopped down to reduce background noise.

DIAL Concepts

The optical receiver was designed primarily to measure atmospheric gases using a differential absorption LIDAR (DIAL) technique originated by Schotland (1974). This method utilizes the narrow bandwidths of the laser and molecular absorption lines. The laser cavity is tuned to alternately fire at the center of an absorption line and at a wavelength just outside of the absorption curve. The intent of the differential absorption technique is to isolate the absorption of the laser radiation by the gas under study from all other sources of attenuation. DIAL assigns as a baseline

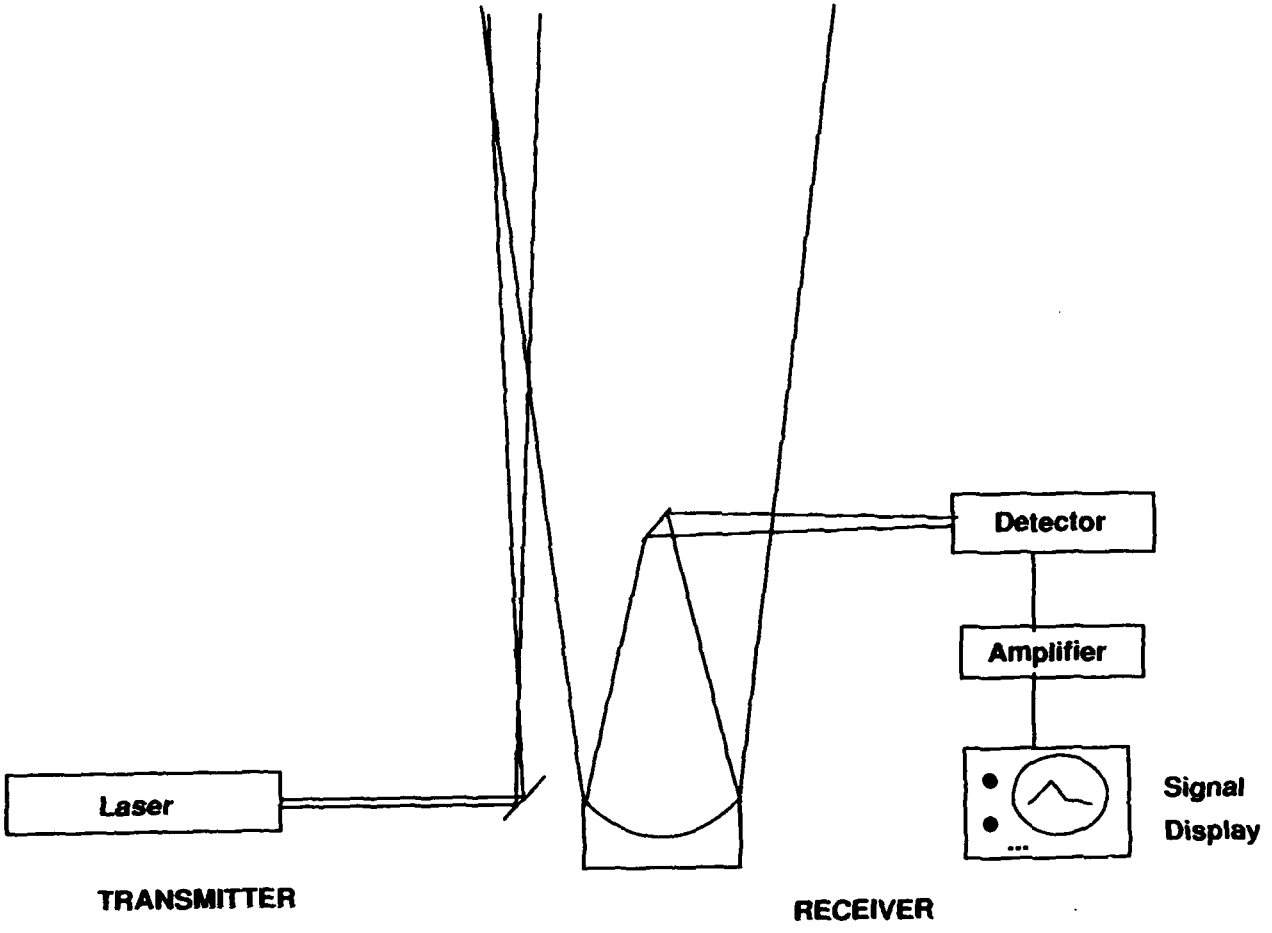

Figure 2.0 Biaxial Monostatic LIDAR System

the backscattered laser induced radiance from the atmospheric gases of the sky at a wavelength near, but outside the absorption bandwidth of the species being investigated. The difference between the backscattered signal of the two wavelengths is attributed solely to absorption by the molecule or aerosol in question.

This is a very effective method of subtracting the atmospheric background noise. However, the scattering properties of the atmosphere are highly time and wavelength dependent. Therefore, measurements must occur in very short time intervals and at small wavelength differences.

Unwanted sky radiance is reduced in the receiver by placing narrow bandpass filters in front of the photomultiplier tube. These filters will only transmit light within a narrow wavelength interval centered on the resonant frequency of the laser cavity. The return signals are then compared to the output radiation of the laser.

Many factors affect the degree of scattering and absorption of light as it passes through the atmosphere. We employ the LIDAR equation to help us identify the various contributions to the backscattered signal. The next section contains a simplified derivation of the general form of the LIDAR equation. It closely follows a more detailed discussion in Measures (1984).

LIDAR Equation

The interpretation of a backscattered signal is not entirely unambiguous. The signal at the detector is an integrated return from the entire volume within the solid angle of the instrument's field of view. This is a two-fold problem. First, we are observing the radiance of a large portion of the volume that does not interest us. Secondly, the intervening atmosphere

between object and observer is attenuating the laser radiation on both the uplink and the downlink paths. We must look for ways to isolate that portion of the signal which is of most interest to us - a narrow scattering volume at a range R.

The LIDAR equation helps us extract the various attenuation effects within the scattering volume. As in most other things, mathematically it may be expressed quite simply in integral form. Unfortunately, hidden in the mathematical representation is a great deal of uncertainty. The LIDAR equation as written below is the most general form for elastic or inelastic collisions, applicable to a pulsed, monostatic LIDAR (Measures, 1984). The total signal power arriving at the detector at an instant t is expressed by:

$$P(\lambda,t) = \int_0^{R=ct/2} dR \int_{\Delta\lambda_o} d\lambda \int J(\lambda,R,r)\; p(\lambda,R,r)\, dA(R,r) \qquad \text{(eq 1)}$$

The terms $J(\lambda,R,r)$ and $p(\lambda,R,r)$ though simply written are quite complex. The latter represents the probability that radiation of wavelength λ that was emitted from the position radius r in the target plane and located at a range R from the receiver will strike the detector. Many factors influence this probability. It is rewritten below in a form that contains geometrical considerations, atmospheric attenuation, the receiver optics and spectral transmission characteristics:

$$p(\lambda,R,r) = \frac{A_o}{R^2}\, \xi(\lambda)\; \xi(R,r)\; T(\lambda,R) \qquad \text{(eq 2)}$$

In this equation three terms are readily known. A_o/R^2 is the acceptance solid angle of the receiver, where A_o is the area of the objective lens or mirror. $\xi(\lambda)$ represents the receiver's spectral transmission efficiency. Thirdly, $\xi(R,r)$ is the probability of radiation from position r in the target plane and at a range R from the receiver ever reaching the detector, based solely on geometrical considerations. All three are computed from numbers that are easily measured and can therefore be known to a high degree of accuracy.

The last term, $T(\lambda,R)$, incorporates atmospheric losses along the downlink path to give us transmittance, and is usually written as:

$$T(\lambda,R) = \exp\left[-\int_0^R \kappa(\lambda,R)\,dR\right] \qquad \text{(eq 3)}$$

This is the atmospheric transmissivity at wavelength λ calculated at a range R from the receiver. The attenuation coefficient, κ, is often computed by modeling the atmosphere. It is not calculated as an exact number, but usually an order of magnitude approximation.

Returning to Equation 1, we see that $J(\lambda,R,r)$ is the laser induced spectral radiance at wavelength λ and at position r in the target plane located at a range R from the receiver. This is the amount of light which reaches the target and gets backscattered. It is usually written in the following form:

$$J(\lambda,R,r) = \beta(\lambda_L,\lambda,R,r)\; I(\lambda_L,R,r) \qquad \text{(eq 4)}$$

The interaction between the laser radiation and the target medium is presented as the volume backscattering coefficient $\beta(\lambda_L, \lambda, R, r)$. This coefficient is the term we need to solve for to determine aerosol densities. Note that λ_L is the laser linewidth, while λ is integrated across the bandwidth of the receiver. To see this more clearly, the volume backscattering coefficient can be rewritten as a summation:

$$\beta(\lambda_L, \lambda, R, r) = \sum_i N_i(R, r) \left\{ \frac{d\sigma(\lambda_L)}{d\Omega} \right\}_i \mathcal{L}_i(\lambda)\Delta\lambda \qquad \text{(eq 5)}$$

The term of interest, $N_i(R, r)$ is the number density of a scattering species at position r in the target plane and at a range R from the receiver. The differential scattering cross section when irradiated by a laser at wavelength λ_L is $\left\{ \frac{d\sigma(\lambda_L)}{d\Omega} \right\}_i$. $\mathcal{L}_i(\lambda)\Delta\lambda$ gives a Lorentzian line distribution to the backscattered light due to the molecular motion of the atmosphere. It is usually treated as a delta function because it is much smaller than the receiver's spectral window $\Delta\lambda_o$. This leaves us with the final question of how much radiation actually arrived at the target in the first place.

The last term of Equation 4, $I(\lambda_L, R, r)$ is the laser irradiance at position r and range R from the receiver. As stated above, in order to know this number we must determine the total atmospheric attenuation of the beam along the entire uplink path. This is not easily done. There are, however, a number of fairly reliable computer models which give reasonable answers and are generally used.

DIAL Equation

The differential absorption LIDAR technique, as discussed earlier, uses two laser pulses separated in wavelength by a small amount and compares the difference in atmospheric attenuation between them. The first wavelength, λ_o, corresponds to the center of a strong absorption line of strength κ_o for an aerosol or molecule of interest. The second wavelength, λ_w, lies in the wing of the absorption line of strength κ_w. We calculate the difference in atmospheric attenuation between these wavelengths by taking the ratio of the two return power signals, assuming that the output power is the same for both.

$$\frac{P(\lambda_o,R)}{P(\lambda_w,R)} = \frac{\xi(\lambda_o)\,\beta(\lambda_o,R)}{\xi(\lambda_w)\,\beta(\lambda_w,R)}\,\exp\left[-2\int_0^R \{\kappa(\lambda_o,R)-\kappa(\lambda_w,R)\}\,dR\right] \quad \text{(eq 6)}$$

We must now make the assumption that the difference in attenuation is solely a function of absorption by the species we are investigating, and separate that absorption from the total attenuation coefficient:

$$\int_0^R N(R)\;\sigma_A(\lambda_o{:}\lambda_w)\,dR = \frac{1}{2}\ln\left[\frac{P(\lambda_w,R)\,\xi(\lambda_o)\,\beta(\lambda_o,R)}{P(\lambda_o,R)\,\xi(\lambda_w)\,\beta(\lambda_w,R)}\right] - \int_0^R \{\bar{\kappa}(\lambda_o,R)-\bar{\kappa}(\lambda_w,R)\}\,dR \quad \text{(eq 7)}$$

Here $N(R)$ is the number density of the species at range R, and $\sigma_A(\lambda_o{:}\lambda_w)$ is the differential absorption cross section. Next we write the equation in

differential form and solve for $N(R)$:

$$N(R) = \frac{1}{2\,\sigma_{\lambda}(\lambda_{\cdot}:\lambda_{w})}\left[\frac{d}{dR}\left\{\ln\left[\frac{P(\lambda_{w},R)}{P(\lambda_{\cdot},R)}\right] - \ln\left[\frac{\beta(\lambda_{w},R)}{\beta(\lambda_{\cdot},R)}\right]\right\}\right.$$

$$\left. + \bar{\kappa}(\lambda_{w},R) - \bar{\kappa}(\lambda_{\cdot},R)\right] \qquad \text{(eq 8)}$$

We can simplify Equation 8 by comparing the relative order of magnitudes for the extinction terms as a function of Rayleigh or Mie scattering. For Rayleigh scattering (molecules), we note that the volume backscattering coefficient, $\beta(\lambda,R)$, will be roughly the same at both wavelengths. That allows this term to approach zero. Similarly, for Mie scattering (aerosols) the atmospheric attenuation coefficients, $\bar{\kappa}(\lambda_{\cdot},R)$ and $\bar{\kappa}(\lambda_{w},R)$, are nearly equal and that term goes to zero. This lets us calculate number density strictly on the basis of backscattering coefficient for aerosols and absorption coefficient for molecules.

In conclusion, the backscattered laser signals can be processed using the LIDAR and DIAL equations, but the assumptions made in solving them should be fully understood.

CHAPTER 3

DYE LASER

Lasers use many media to effect stimulated emission. The laser in this experiment is a coaxial-pumped, dual dye laser (Alejandro, 1983). The laser consists of two separate resonant cavities, each with a different dye solution. The dye flows axially through the center of a Quadrax tube (Figure 3.1) and is radiated by the cylindrical flashlamp.

The Quadrax tube has a central dye cell (A) capped with quartz flats (B) at either end. The quartz walls (C) of the dye cell are evacuated to provide thermal insulation. The dye cell's outer wall is surrounded by a sheath of water (D) to provide cooling and additional insulation. The next concentric cylinder is a Candela CL-1000 zenon flashlamp (E) encased in a metal jacket (F). The flashlamps can discharge up to 900 Joules in a 0.75 microsecond pulse at 1 Hertz (Alejandro, 1983). The metal jacket provides structural integrity and its reflective inner surface helps focus the flash-lamp energy on the dye solution. The metal jacket also has cool water flowing through it to help reduce the flashlamp temperature.

The flashlamp discharges energy into the dye solution in the form of broadband, incoherent light, much like the flash of a strobe light. The wavelength of maximum absorption is dependent on the length of the dye's molecular chain. This energy instantaneously excites the dye to a higher energy state. Over the period of a microsecond, the ensemble coherently returns to lower energy states, with each molecule emitting a photon.

Figure 3.1 Cross Section of Quadrax Tube

Component	Description
A	Dye Cell
B	Quartz Flats
C	Evacuated Quartz Tube
D	Water Sheath
E	Flashlamp
F	Metal Jacket

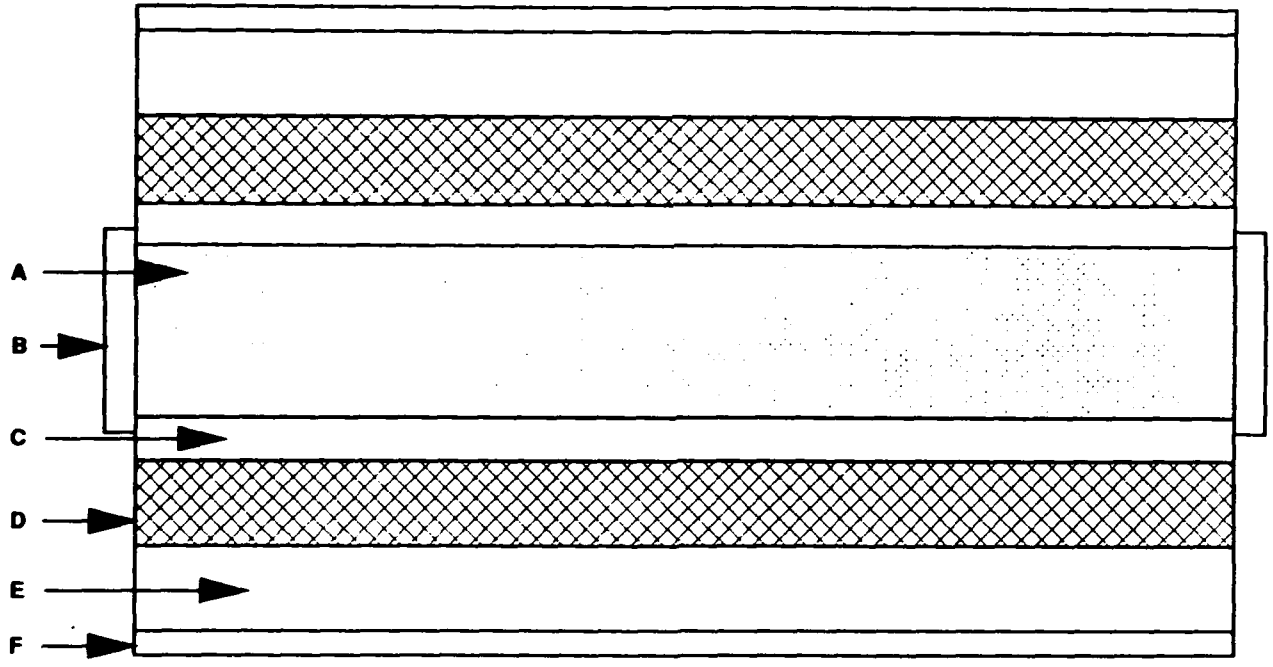

Figure 3.1 Cross Section of Quadrax Tube

Photons centered about the resonant frequency of the cavity are coupled to form the output laser pulse.

Chemistry

The two dyes used in this laser are Coumarin 450 and Rhodamine 6G. Dyes are organic compounds containing conjugate double bonds. The characteristic length of their molecular chains makes them good absorbers of short wavelength energy. As we know, good absorbers also make good emitters. Thus, Coumarin 450 has a peak emission at 460 nanometers, while Rhodamine 6G lases at 580 nanometers. Each of the dyes have a spectral bandwidth of approximately 35 nanometers.

Dye efficiency is dependent both on the solvents used to make a solution and on photo decomposition. The Coumarin 450 solvent is a 1:1 mixture of ethanol and distilled water. The optimum concentration is $1 x 10^{-4}$ moles/liter. Rhodamine 6G is diluted in 100% methanol to a concentration of $4 x 10^{-5}$ moles/liter. Dye efficiency decreases with increased laser use. Also, ambient sunlight in the laboratory appears to degrade dye solutions over time.

The dyes are pumped from large reservoirs under the laser cavity through the dye cell in the Quadrax tubes. This provides a fresh supply of dye molecules to be stimulated during rapid firing sequences.

Resonant Cavity

The resonant cavity (Figure 3.2) consists of a blazed diffraction grating (A) at the rear, a 40% reflective quartz output coupler (B) at the front, two adjustable apertures (C) for alignment of the beam, and the

Quadrax tube (D) in between. The output wavelength of the laser is dependent on the angle of the diffraction grating to the optic axis. The first order reflection is coupled through the laser cavity by adjusting this angle. The gratings sit on a two-position mount that is manually adjusted. The rotational adjustment screws are fitted with micrometer barrels which are calibrated to read out wavelength directly in nanometers.

Light transmitted by the output coupler is collimated to reduce beam divergence to 4 milliradians. Output beams from the collimators (E) are directed to the transmitter's steering mirror. The steering mirror directs the beam through the roof hatch and into the sky within the receiver's field of view.

Figure 3.2 Resonant Cavity

Component	Description
A	Blazed Diffraction Grating
B	Quartz Output Coupler
C	Variable Iris Aperture
D	Quadrax Tube
E	Beam Colimator

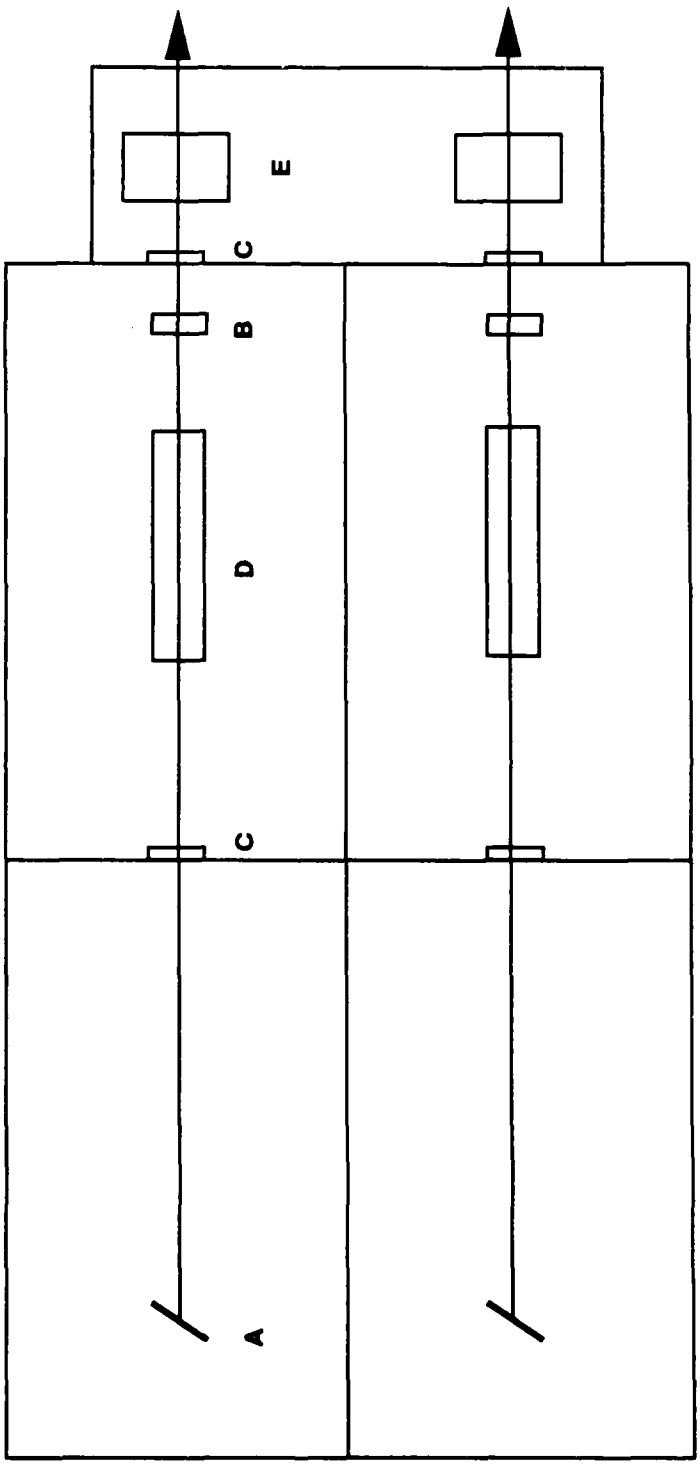

Figure 3.2 Resonant Cavity

CHAPTER 4

THE TELESCOPE

The telescope is the most massive part of the receiving system. In the final design stage, the telescope was constructed in a Newtonian fashion. The primary mirror collects backscattered laser light from the atmosphere and the secondary mirror directs the signal to the lens at the entrance of the detector assembly. This lens acts as an eyepiece of the telescope and focuses the full aperture of the primary mirror onto the cathode of the photomultiplier tube. Only rays which arrive nearly parallel to the optic axis enter the receiving system.

The Tower

The first step of building the telescope was to establish a sturdy mounting platform for the individual optic elements. The roof of the Physics and Atmospheric Sciences building had two small cement pads available from a previous experiment. They were located only seven feet from the optic axis of the transmitter and thus were very suitable for the receiver base. The primary mirror was placed on one pad and a tower was erected around it for mounting the secondary mirror and detector assembly.

The tower was constructed with 1.5-inch angle iron bolted together like an erector set. The base was anchored to the cement pads with lag bolts and lead expansion shields. The tower has an internal chamber three feet square and ten feet high. This extra height permits me the flexibility of

mounting my detector overhead at the focal point of the primary mirror in future experiments. The framework to support the two foot long detector assembly directly overhead, and the subsequent occulting of the primary mirror were unacceptable for this project. It is also much easier to service the detector assembly and shield it from the elements when it is mounted off to one side.

The Primary Mirror

The aperture of the receiving system is the 30-inch diameter, primary mirror of the telescope. This is the entrance pupil through which backscattered radiation is collected, and then focused onto the cathode of the PMT. Field stops placed in front of the eyepiece lens can be used to reduce the total field of view. When the system is wide open, the receiver has a 9 milliradian field of view.

The mirror was cut from a 1.625-inch glass slab and parabolically ground to a 96-inch focal length (f/3.2). This means it is a fairly fast camera which is necessary given the relatively low light levels it will be sensing. Since this is such a large optical element it needs a sturdy mount and rugged external protection. A nine-point suspension system was bolted to the cement pad to mount this mirror. This nine-point suspension is about half the requirement for an imaging system.

The suspension system is composed of three mounting brackets. Each bracket (Figure 4.1) consists of a triangular plate (A) , a lever arm (B), a fulcrum (C), an adjustment nut and bolt (D), and a base plate (E). Three plastic buttons (F) are glued to the top surface of each triangular plate to

Figure 4.1 Suspension Mounting Bracket

Component	Description
A	Triangular Plate
B	Lever Arm
C	Fulcrum
D	Adjustment Nut and Bolt
E	Base Plate
F	Plastic Buttons
G	Nipple
H	Mirror

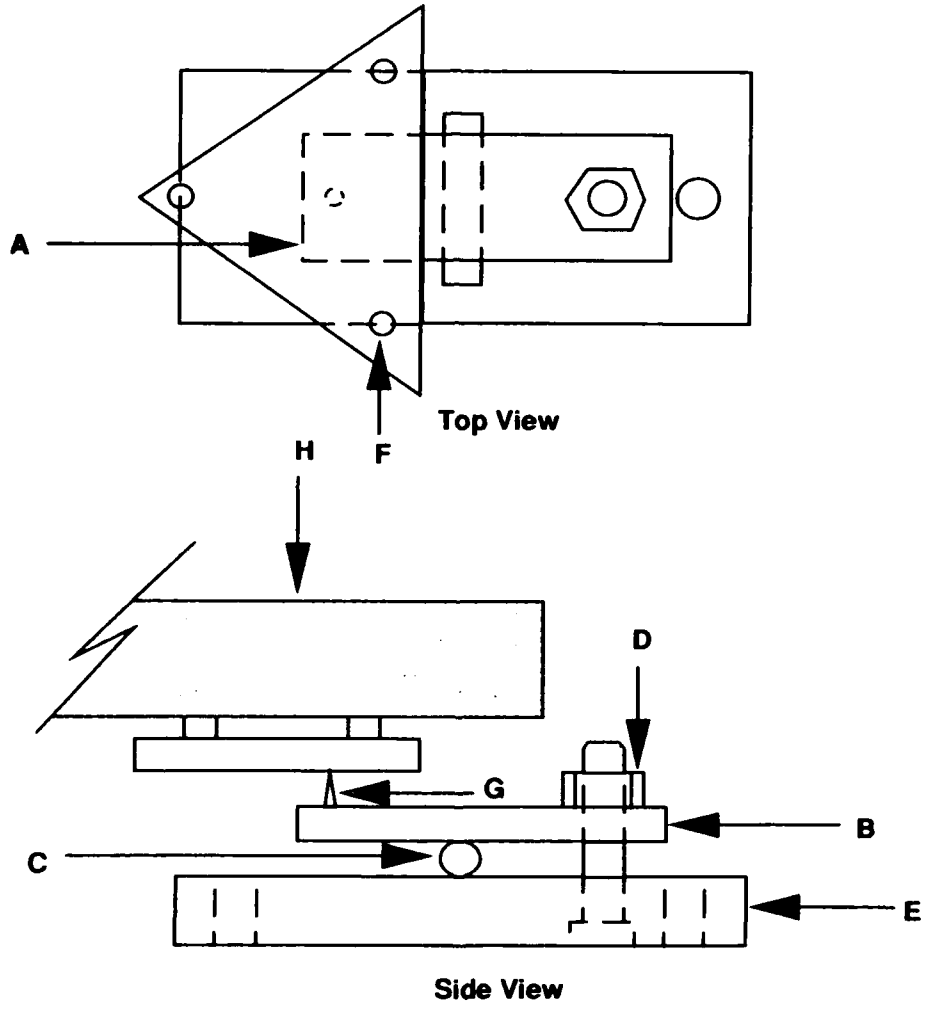

Figure 4.1 Suspension Mounting Bracket

provide a total of nine suspension points. The triangular plates are balanced on a nipple (G) at the end of each lever arm. The opposite end of the lever arm is attached to the base plate by an adjustment nut and bolt. A cylindrical fulcrum separates the lever arm from the base plate. The weight of the mirror (H) is distributed across the fulcrum and the adjustment nut and bolt. The mirror is leveled by tightening or loosening these adjustment nuts.

The primary mirror is protected from the elements by a box enclosure. The sides of the box are made from 0.75-inch pine boards, and the cover from 0.25-inch sheet aluminum (Figure 4.2). The pine boards were first painted and then bolted to the cement pad with L-shaped brackets and lag bolts. The bottom edge of the boards are sealed to the cement pad with butyl-type caulking on both sides to prevent the intrusion of dust and sand.

The aluminum cover overlaps the pine boards on all sides and is secured by four small trunk latches. A 0.75-inch thick piece of weather strip was glued to the inside of the cover. It is compressed between the top of the boards and the cover to prevent blowing sand from entering the enclosure. Two handles are attached to the top of the cover for easy lifting. The cover can be hung on the side of the tower by these handles when the system is in use.

Figure 4.2 Primary Mirror Enclosure

Component	Description
A	Aluminum Cover
B	Pine Board Sidewall
C	Primary Mirror
D	Mounting Bracket

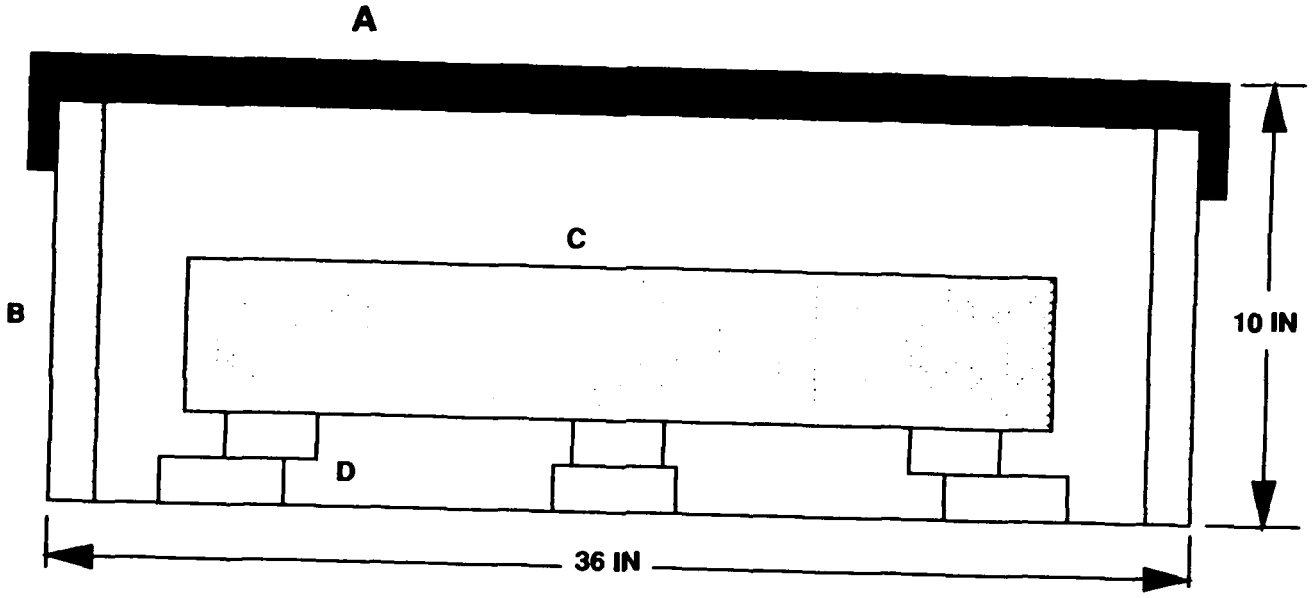

Figure 4.2 Primary Mirror Enclosure

The Secondary Mirror

The secondary mirror functions solely as a steering device. It directs light received by the primary mirror to the detector assembly. The optic path is bent 90 degrees to the vertical with the focal point of the primary mirror at a distance of two feet from the centerline. This positions the detector assembly outside the field of view of the primary mirror. The secondary mirror and its mounting assembly are the only objects which obscure the receiver's field of view.

The secondary mirror is a flat, front-surfaced, rectangular mirror (5 inches by 7 inches). It is centered on the optic axis at an angle 45 degrees to the vertical and 72 inches above the surface of the primary mirror. The materials used to mount the secondary mirror were kept to the lightest weight and minimum size. Obscuration of the primary mirror by the secondary mirror and its mounting assembly is approximately five percent.

The mounting bracket for the secondary mirror (Figure 4.3) was machined from aluminum blocks. It is attached to a piece of angle iron stretched across the center cavity of the tower. The mounting bracket permits adjustment of the secondary mirror along three orthogonal axes. This is necessary during initial alignment of the system. Vibration of the secondary mirror may become a problem at wind speeds greater than 30 mph. However, at that wind speed one would also risk damage to the primary mirror surface by blowing sand. A dust cover protects the secondary mirror from the elements when the system is not in use. The dust cover is attached by thumb screws at the top and bottom of the bracket.

Figure 4.3 Secondary Mirror and Mounting Bracket

Component	Description
A	Secondary Mirror
B	Three Point Adjustment Plate
C	Mounting Bracket
D	Angle Iron Attached to Tower

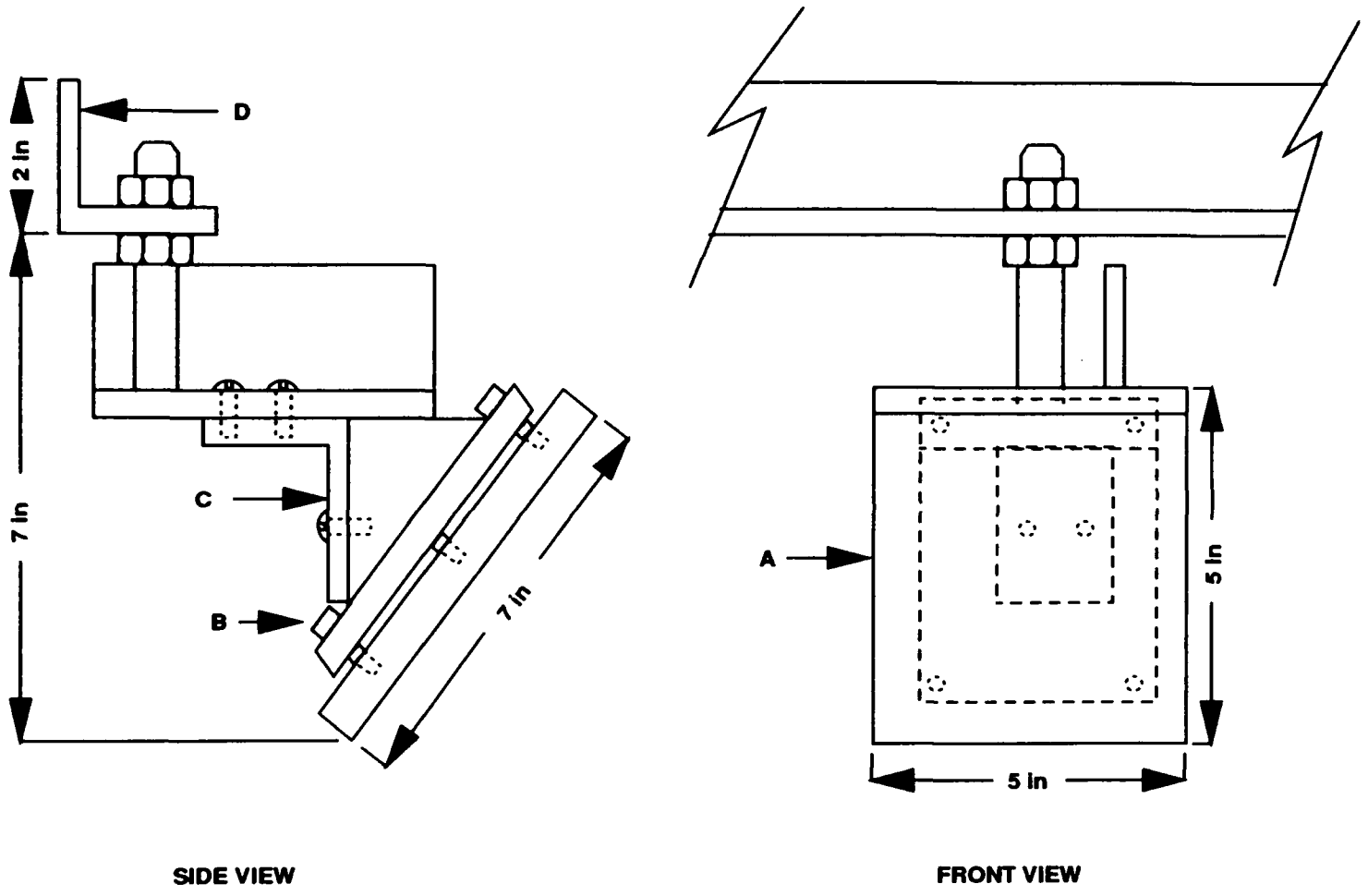

Figure 4.3 Secondary Mirror and Mounting Bracket

CHAPTER 5

DETECTOR ASSEMBLY

The detector assembly is the heart of the optical receiver. It is housed in a light-tight aluminum box. The detector assembly contains three major optical components: the eyepiece lens, the filter wheel assembly, and the photomultiplier tube. Light directed from the secondary mirror passes through a fixed aperture before striking the eyepiece. This lens focuses the light through a bandpass filter and images the primary mirror onto the cathode of the PMT. An amplified output signal is transmitted by the PMT to be displayed on an oscilloscope.

The Eyepiece

The eyepiece is a lens whose focal point is located at the focal point of the primary mirror and centered on the optic axis. The lens is a 1.5-inch diameter, silicon-quartz, planar convex lens with a 100 millimeter focal length. In front of and against the lens is a one-inch diameter fixed aperture called the field stop. This limits the angular distance from the vertical that the primary mirror can collect light and transmit it to the PMT. Once the system is aligned, a set of smaller diameter field stops are available to restrict the field of view. Within its field of view, the system measures the total light intensity per unit time.

The telescope is not designed to image an object at a distance, but rather to measure the total energy incident on the primary mirror. This is

done by imaging the primary mirror, onto the photomultiplier tube. Light received in the field of view is distributed across the surface of the cathode. The detector output signal is proportional to the number of photons striking the detector per unit time. The energy entering the telescope as a function of time is then related to the atmospheric backscatter cross section as a function of height in the atmosphere.

Bandpass Filters

The sky radiance is always present in the form of broadband background radiance, especially strong at visible wavelengths during daytime hours. Not all sky radiance can be deleted by reducing the field of view. Therefore, one must attempt to limit the wavelength interval in which the receiver operates. Operating within a very narrow wavelength interval can be accomplished with narrow bandpass filters.

As the name implies, bandpass filters only transmit light within a predetermined bandwidth. Other wavelengths are either reflected out of the path or absorbed by the filter. The pass band is ideally centered on the resonant frequency of the laser and only slightly wider than the full-width laser pulse. The spectral width of the laser is approximately 0.15 Angstroms (Alejandro, 1983).

The receiver uses bandpass filters with a 10 Angstrom full-width, half-power transmission profile. This means that the fifty percent relative transmittance is 5 Angstroms on either side of the central wavelength. Relative transmittance because the filter itself attenuates the signal. The absolute transmittance of the central wavelength may be as low as

15-20 percent. Figure 5.1 gives the relative transmittance curve for one of the bandpass filters used on this project.

The bandpass filters are mounted on a wheel to facilitate rapidly changing them as the wavelength of the LIDAR is changed. The wheel will accommodate up to six 1-inch diameter filters (Figure 5.2). Filters positions can change at the rate of once every three seconds. The filter wheel is belt driven by a small electric motor connected to the rotation shaft.

Each of the six filter positions is identified by a three digit code. On one side of the wheel are three LED lamps with three PIN diodes on the opposite side which act as receivers. In front of each LED the wheel may or may not have a hole drilled. The presence or absence of light either turns on the diode or leaves it at ground. This is interpreted by the computer as a digital message uniquely identifying the filter position. When the correct filter is in place, the electric motor is turned off. Positive alignment is accomplished with a ratchet relay switch. This prevents misalignment due to wheel inertia by locking the filter position in the center of the optic path.

The Photomultiplier Tube

The photomultiplier tube is a photoelectric device used to convert radiant energy into electrical signals. The PMT produces an amplified output signal at a gain of four to six orders of magnitude greater than the input signal. Photons arriving at the PMT strike its cathode and release electrons. These electrons cascade down a series of charged plates that release even more electrons. Thus, in an avalanche fashion, each photon produces a voltage at the output of the PMT. The output signal is

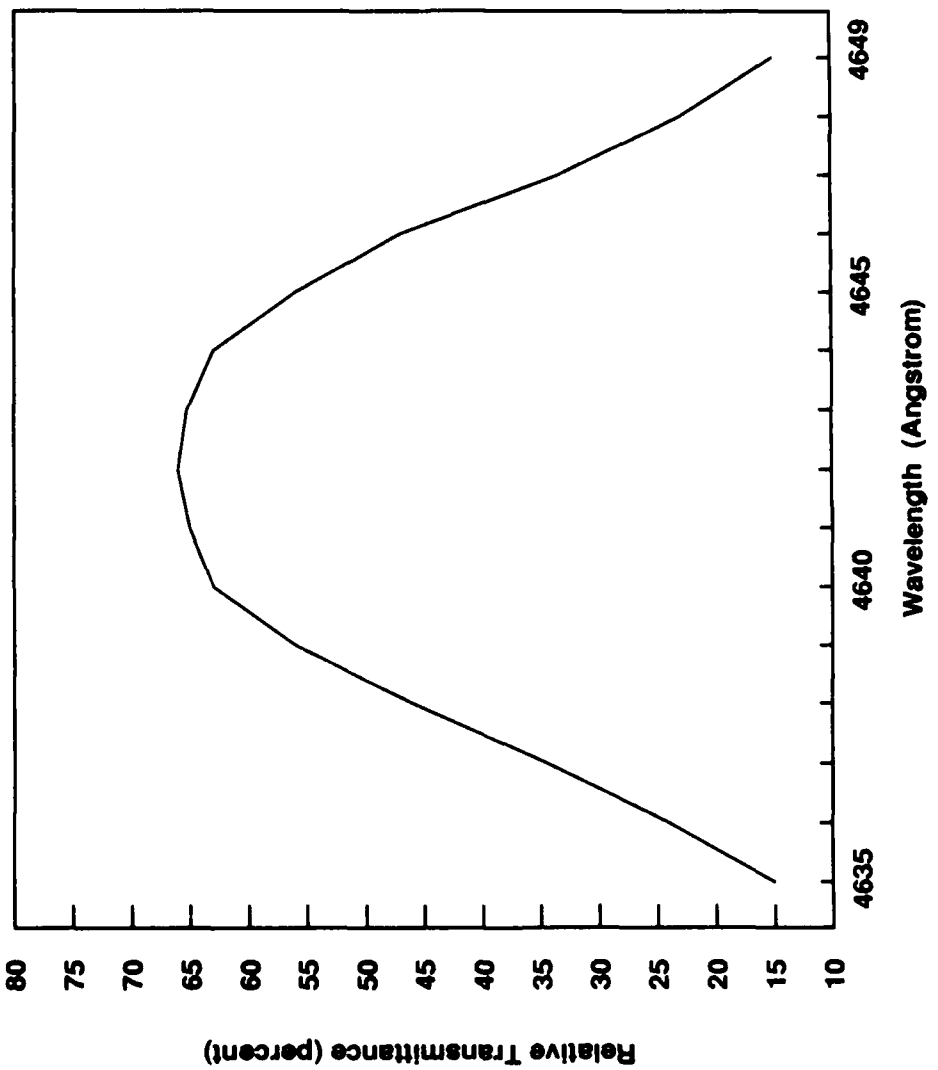

Figure 5.1 Bandpass Filter Transmittance Curve

Figure 5.2 Bandpass Filter Wheel Assembly

Component	Description
A	Filter Wheel Carousel
B	Bandpass Filter
C	Drive Gear
D	Electric Drive Motor
E	Light Emitting Diode
F	Detector

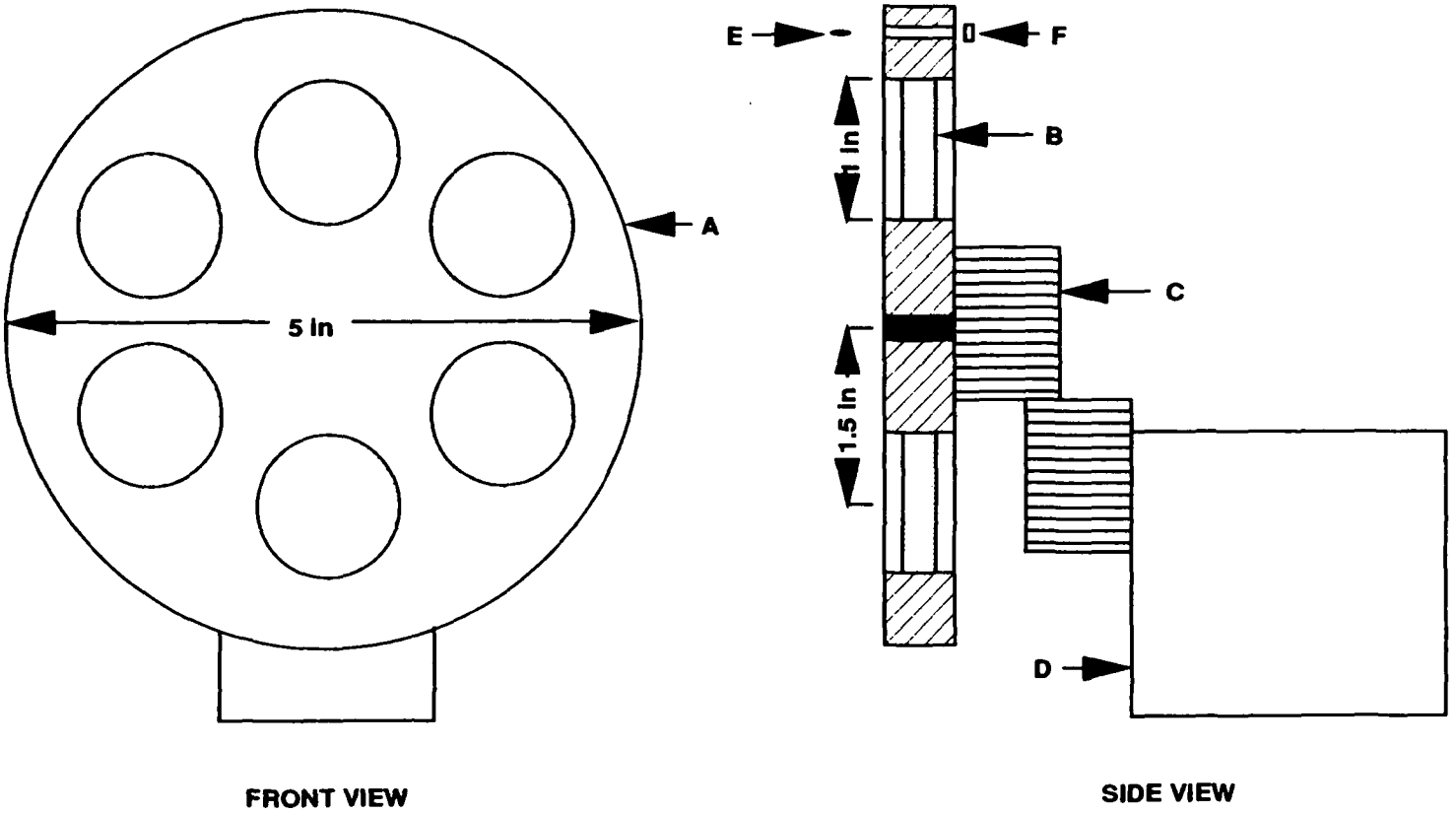

Figure 5.2 Bandpass Filter Wheel Assembly

proportional to the number of photons which strike the cathode. Performance characteristics may vary greatly depending on the type of photomultiplier tube used.

The receiver uses a Thorn EMI 9558QB type tube which has an S-20 (trialkali) photocathode. It has a spectral range from 1650-8500 Angstroms which peaks near 4000 Angstroms. At the wavelength intervals being investigated, the tube has a quantum efficiency of 15 to 17 percent.

The PMT is a cylindrical tube 2 inches in diameter and 5.5 inches long. It is plugged into a circuit board which contains a line amplifier to boost the output signal before sending it to the oscilloscope. The PMT and the line amplifier are suspended inside a 0.25-inch aluminum cylinder three inches in diameter and one foot long (Figure 5.3). Both devices are electrically isolated from the aluminum cylinder.

The PMT and line amplifier together produce about 4 watts of heat or 13.7 BTUs per hour. This heat produces thermal currents in the chamber. The air temperature around the PMT is maintained at room temperatures by thermally isolating the aluminum cylinder from the rest of the assembly and the outside environment. Then a thermoelectric heat pump is used to maintain the desired internal temperature.

Heat Pump

A thermoelectric heat pump, also known as a Peltier pump, is a solid state device that uses electron flow to transfer heat. The pump consists of two pieces of semiconductor material connected in series to a D.C. power source. As Figure 5.4 indicates, one-half of the pump has n-type (negative)

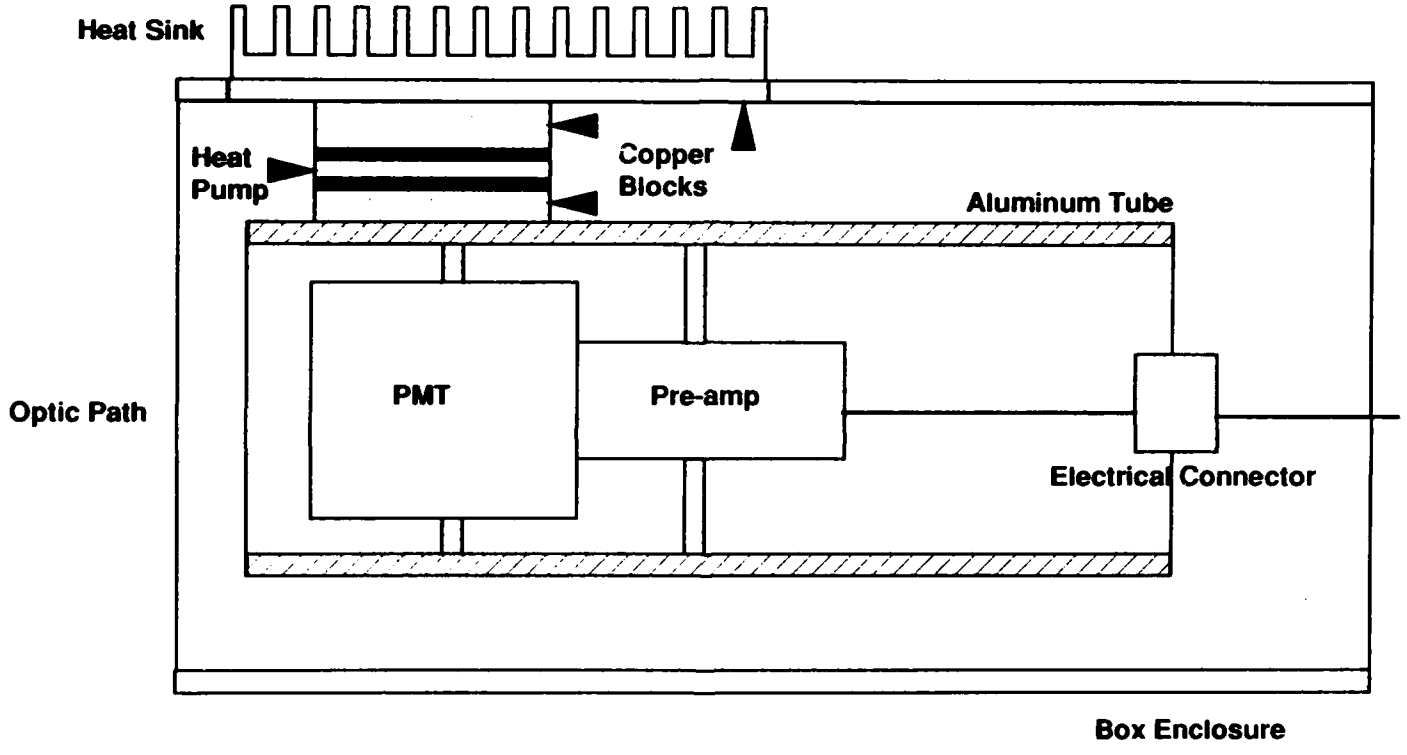

Figure 5.3 Detector Assembly

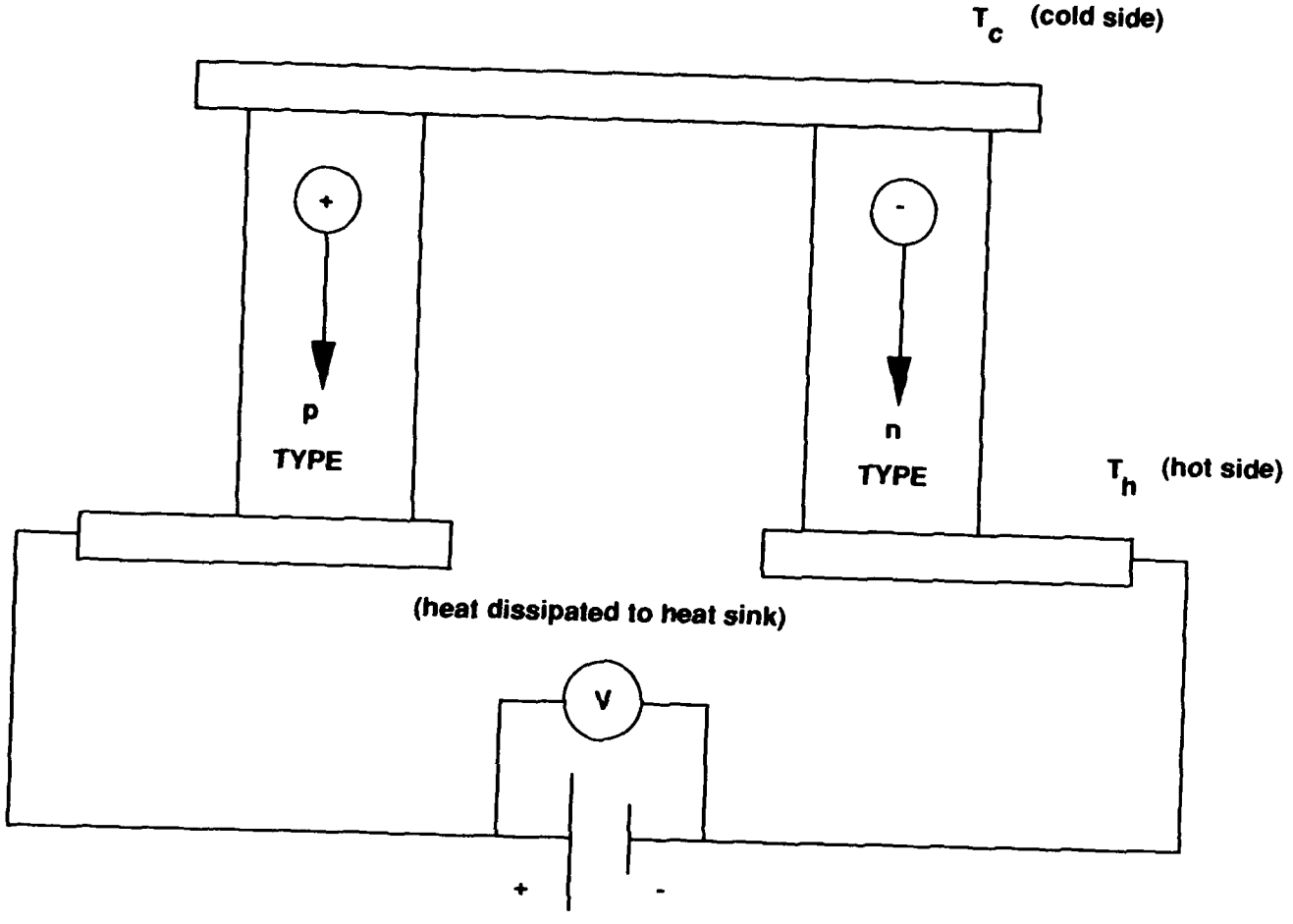

Figure 5.4 Diagram of a Thermoelectric Heat Pump

semiconductor material while the opposite side is made of p-type (positive) material. The tab connecting the two semiconductors provides the surface through which heat is exchanged.

The pump may act as either a cooling or a heating pump depending on the direction the current flows through the device. Cooling is accomplished when a D.C. current passes from the n-type to the p-type material. As the current flows through the semiconductor material, the temperature T_C of the interconnecting tab decreases and heat is absorbed from its surroundings.

Cooling of the tab occurs because the electrical current creates a flow of electrons from the low energy level in the p-type material through the tab to a higher energy level in the n-type material. These electrons absorb energy from the tab as they pass through the material, and decrease its temperature. The tab attempts to reach equilibrium with its surroundings by absorbing more heat. This cycle continues and allows the absorbed heat to be conducted through the semiconductor material by electron transport. At the opposite junction the temperature T_H increases and the heat is liberated as the electrons return to a lower energy level in the p-type semiconductor material. This hotside junction then dissipates the heat through a heat sink.

The heat pump was sandwiched between two blocks of copper. Copper was employed because of its excellent thermal conductivity. The first surface is thermally connected to the aluminum tube surrounding the PMT housing. The second surface is set into the cover of the detector assembly box. Next, a heat sink was attached to the exterior copper plate to

dissipate the heat. Later a small fan was added to increase the airflow across the heat sink, and a small hood was placed around it to channel the airflow and prevent direct solar heating. This increased the efficiency of the heat sink considerably.

The heat pump is rated for 75 watts, but produces nearly 20 watts itself during this process, and the PMT assembly only produces 4 watts when energized. With an outside air temperature of 85°F, it was able to maintain a chamber temperature of 60°F with the heat pump operating at one-third capacity.

CHAPTER 6

OPERATION

The control electronics for both the laser and the receiver must be fully integrated (Fig 6.1) for the LIDAR to operate effectively. The trigger pulse for the laser is the reference time to which the rest of the system is synchronized. A precise time reference is necessary to accurately measure the distance the beam travels through the atmosphere.

Transmitter

The laser trigger pulse unit is energized by a handheld push button. The first click of the button starts charging the high voltage capacitor from the high voltage power supply to approximately 25 kilovolts. The second click of the button initiates a trigger pulse that discharges the capacitors through the flashlamp and into the dye mixture.

Receiver

The leading edge of the laser trigger pulse also activates the PMT by initiating a one millisecond pulse which gates ON the voltage to the PMT. Initially, the sky radiance is viewed without firing the laser, but energizing the photomultiplier tube. The late afternoon sky in October had a background radiance level of 2 millivolts on the oscilloscope display. This baseline measurement is subtracted from the LIDAR return to obtain an absolute value of the backscattered laser signal.

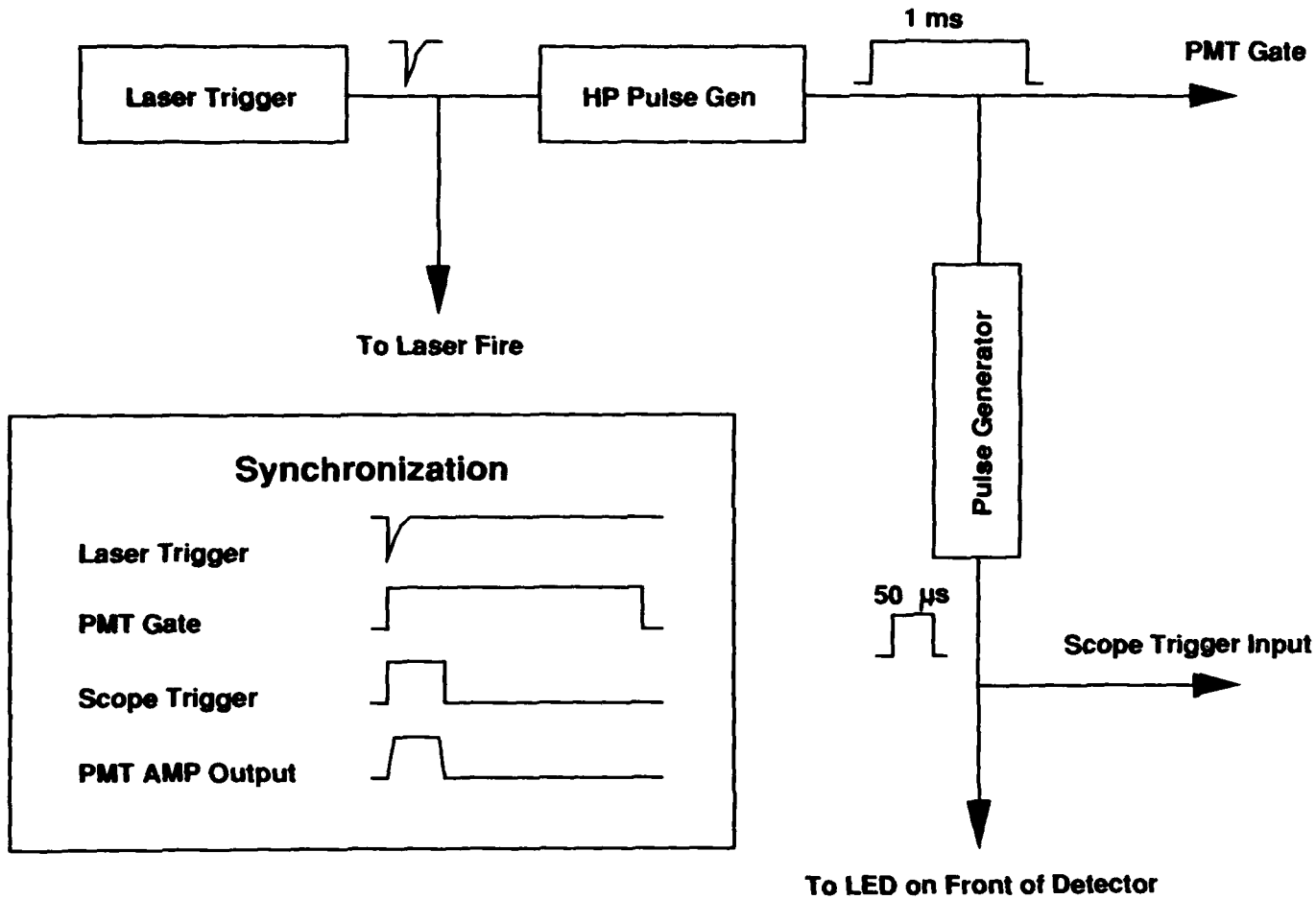

Figure 6.1 Control Electronics

Signal Display

The oscilloscope used to display the returned signals was also synchronized to the laser trigger pulse by a second pulse generator. This generator sent a 50 microsecond pulse to trigger the oscilloscope circuit. The input signal from the PMT was again boosted by a logarithmic amplifier at the oscilloscope to provide enough signal for display, and to decrease the dynamic range of the displayed signal.

The oscilloscope display is also used for final alignment of the system. This was accomplished by adjusting the transmitter's steering mirror while pulsing the laser, and monitoring the oscilloscope. In this way we could visually determine the strongest backscattered signal. Figure 6.2 is a photograph of a backscattered pulse after the system was aligned. The horizontal scale is 10 microseconds per division. This gives an altitude of nearly 15 kilometers for the return.

Note the absence of a signal return on the leading edge of the pulse. This is because the laser beam is outside of the field of view of the receiver. This is an intentional design feature of the biaxial configuration. The benefit is avoidance of the near-field backscattered radiation. Near-field backscatter is normally so intense that the photodetector becomes saturated. Gating ON/OFF of the detector voltage is also used to minimize this problem. The backscattered signal level gradually increases until the laser beam is fully within the receiver's field of view. The signal level decreases with altitude, a function of molecular and aerosol densities which also decrease with altitude, transmittance losses, and energy loss by the inverse square law.

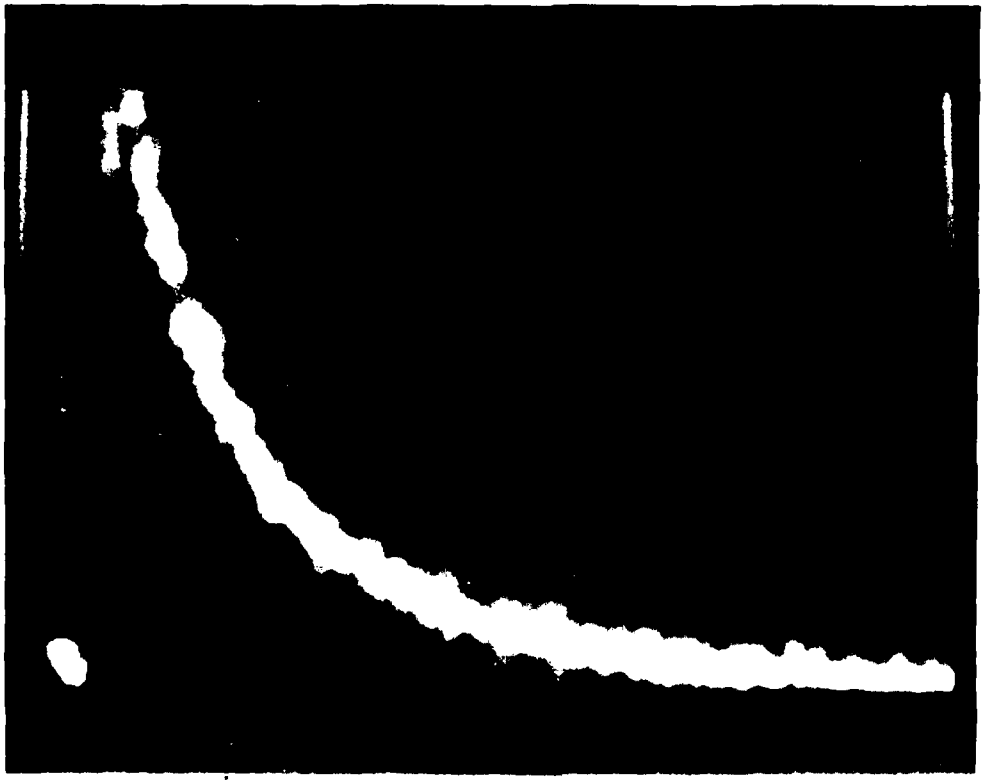

Figure 6.2 Oscilloscope Display of Backscattered Radiation

CHAPTER 7

LESSONS LEARNED

Hindsight is always 20/20, and after completing the experiment I found many items that could have been done differently. Some are nice to have while others impact operation more directly. Fortunately, the operational procedures were sound, so no comments are made on the safety of operation.

Laser Cavity

Contamination of the dye solutions and cavitation appear to be chief irritants. Replumbing the system with threaded joints wrapped in teflon tape is recommended. The glued joints are thought to be a prime source of contamination of the dye solutions. Also, the plumbing system should be designed with fewer elbows to reduce cavitation problems. In addition, the dye reservoirs should be enclosed to reduce the risk of photodecomposition by ambient sunlight.

A problem exists with the calibration of the barrel micrometers on the blaze grating (C-450) or the bandpass filter. During the experiment the barrel micrometer had to be selected 25 nanometers from the central frequency of the bandpass filter for the signal to be observed. Obviously one or the other is incorrectly calibrated. Since bandpass filters are usually calibrated very accurately, the barrel micrometer is suspected to be in error. Unfortunately, there was not enough time to identify which one was at fault.

Optical Receiver

Happily the telescope and detector operated as designed. Unfortunately, using quartz window "E" (Figure 1.4) as a field stop was the result of an error in the original computation. The window should be located 75 millimeters from the relay lens and 55 millimeters from the PMT cathode. This would permit full use of the 0.85 inch active region of the cathode and makes the relay lens the field stop for the system. If the detector assembly was then positioned at 100 inches from the primary mirror, the system would have a field of view up to 15 milliradians. The nice to haves include placing a white canvas awning over the detector assembly to shield it from direct solar radiation. This could also be incorporated into a hood that provides total protection to the detector assembly from dust, rain and other weather elements.

Electronics

Here there is much room for improvement. The entire experiment could be automated with existing equipment in the laser laboratory. The PDP 11/23 can be used to fire the laser and store data files. The Biomation and auxiliary equipment would then be used for signal processing before storage in a computer file. Automating the system is a requirement to get the fidelity necessary to make DIAL measurements. These are steps in the long range plan of this project but not within the scope of my experiment.

Alignment

The process of aligning the optical axes of the receiver and transmitter (Appendix A) is extremely time consuming, and not very exact.

There are errors in visually determining when the beam is level on the roof, and locating the exact center of the primary mirror. Also, the alignment procedure used only addressed alignment of the optic axis. Focusing of the marginal rays from the primary mirror were not accomplished. This could cause some signal loss at the detector. Since then I have considered the problem and make the following suggestions.

First, vertical alignment of the transmitter should occur as in Appendix A. The receiver, however, does not need to use the HeNe laser beam from the transmitter for alignment. Instead, during the day ambient sky radiance should provide enough light for alignment. A large sheet of white paper could be stretched across the top of the tower and illuminated from above, if this alignment procedure must occur after dark.

In either case, a diffuse light source evenly illuminates the primary mirror. The primary mirror should be leveled with the clinometer and straightedge used in Appendix A. Again the PMT should be removed from the detector assembly and an opaque screen such as tissue paper or waxed paper should be placed at the position of the cathode of the PMT. During daytime alignment one may need a hood draped over the detector assembly. Now, the detector assembly can be slid back and forth until the circle of light is exactly 0.865 inches in radius. Drawing this circle on the opaque screen is recommended. Now, the full surface of the primary mirror is exactly imaged onto the active region of the PMT with considerably more certainty and much less work.

APPENDIX A

ALIGNMENT PROCEDURES

The architecture of the LIDAR system presented some unique alignment problems. The laser cavity and steering mirror are located in a fifth floor laboratory of the Physics and Atmospheric Sciences building. The receiving system is mounted on the roof, one story above the laboratory. The laser fires through a scuttle hole in the ceiling of the laboratory which is approximately seven-feet horizontally from the telescope.

Vertical alignment of the laser beam is accomplished by stringing a plumb bob through two washers (Figure A.1): one located on the roof and the other mounted directly above the beam spot on the steering mirror. The HeNe laser used to align the laser cavity was used to determine the optic axis of the laser. The steering mirror was adjusted until the beam passed through the center of both washers. The same beam was used to align the receiver optics.

A small front surface mirror was mounted to the side of the roof hatch set at an angle of 45 degrees to the vertical with a clinometer. This mirror directed the HeNe beam horizontally across the roof and over the center of the primary mirror. A water level was constructed by using a 20-foot piece of 0.75-inch I.D. tubing filled with water and raised at both ends. The mirror was adjusted so that the HeNe beam was centered on both meniscuses. This served as a baseline for aligning the receiver optics.

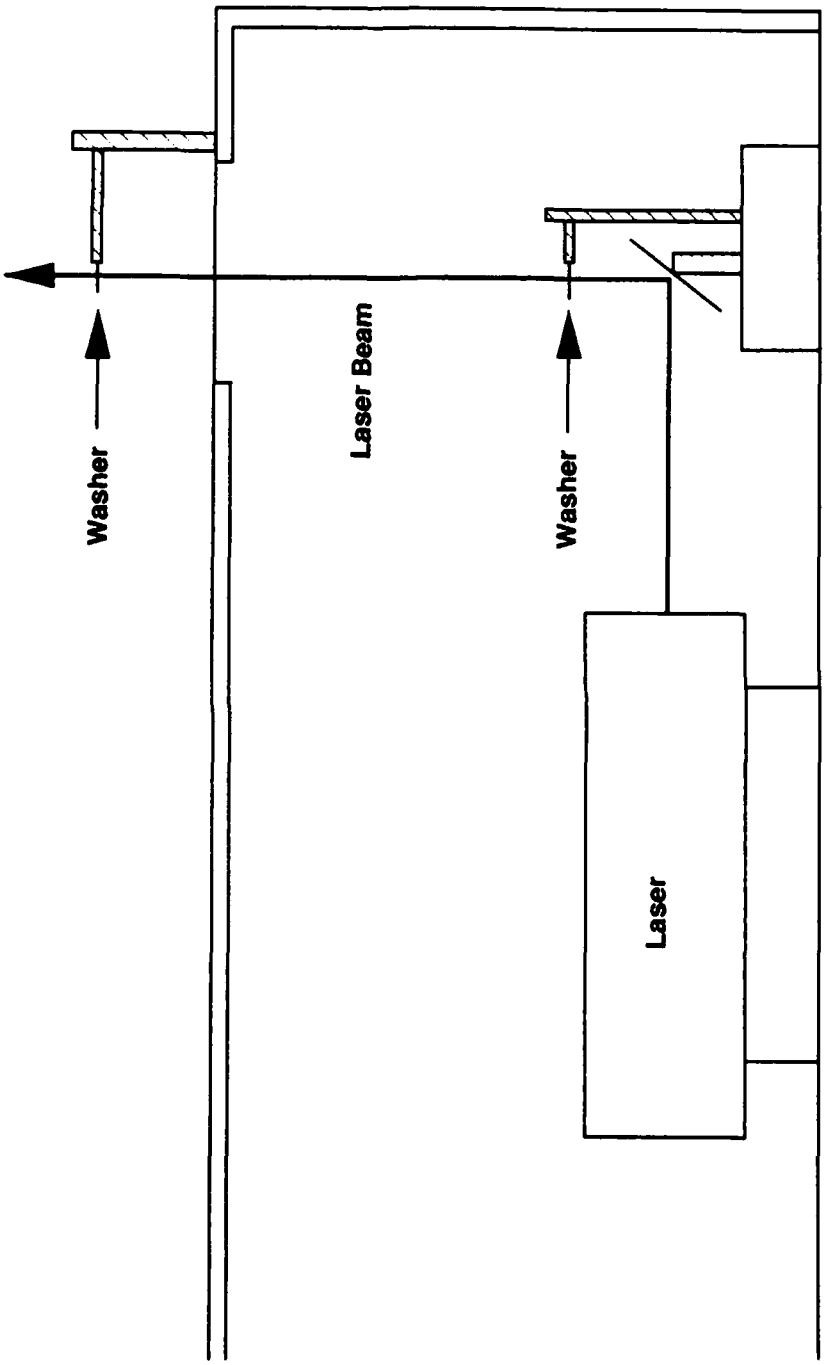

Figure A.1 Vertical Allignment of the Laser Beam

The primary mirror was leveled with a straightedge and a clinometer. A 0.0625-inch thick pane of glass (Figure A.2) was used as a beamsplitter and placed it over the geometric center of the mirror in the HeNe beam's path. The beamsplitter was adjusted until the reflected beam off the primary mirror came back upon itself on the beamsplitter. This vertical beam was used to define the optical axis of the receiving system.

Next, the secondary mirror of the telescope was adjusted to direct the beam through the center of the entrance pupil of the detector assembly. The photomultiplier tube was removed from the assembly and an opaque screen inserted in its place. Final adjust of the secondary mirror was accomplished by centering the reflected beam on the opaque screen. A piece of paper with an outline of the PMT is sufficient to use for a screen. The system is now ready to fire-up.

Normally, the system should see a return signal on the first shot. Final alignment of the system is made by adjusting the steering mirror of the transmitter. The steering mirror is slowly slewed along two orthogonal axes until the strongest return signal is obtained from the receiver.

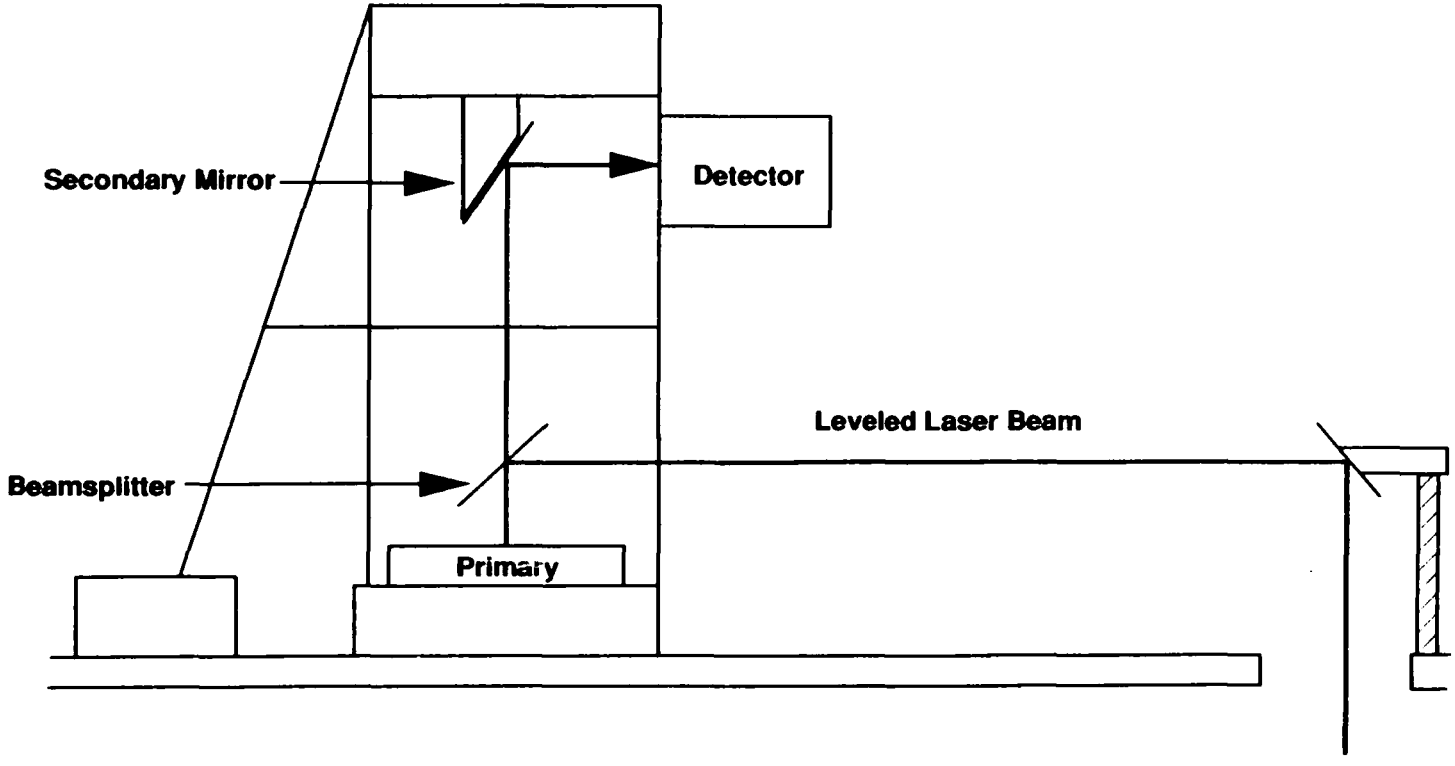

Figure A.2 Vertical Allignment of the Optical Receiver

LIST OF REFERENCES

1. Alejandro, Steven B. (1983), "Development of a Coaxially Pumped Dual Dye Laser System for Lidar Applications," Master of Science Thesis, University of Arizona, Tucson.
2. Jenkins, Francis A. and Harvey E. White (1976), Fundamentals of Optics, McGraw-Hill, New York.
3. Measures, Raymond M. (1984), Laser Remote Sensing: Fundamentals and Applications, Wiley, New York.
4. Schotland, Richard M. (1974), "Errors in Lidar Measurements of Atmospheric Gases by Differential Absorption," J. Appl. Meteorology, Vol 13, 71-77.
5. Wissell, Phillip A. (1983), "Design, Construction and Performance Evaluation of a Gain-Switched Amplifier for LIDAR Applications," Master of Science Thesis, University of Arizona, Tucson.